# Neutron vibrational spectroscopic evidence for short H⋯H contacts in the $R$NiInH$_{1.4;\ 1.6}$ ($R$ = Ce, La) metal hydride

Ryan A. Klein [a,b,∗], Rafael Balderas-Xicohténcatl [c], Jan Petter Maehlen [d], Terrence J. Udovic [b,e], Craig M. Brown [b,f], Robert Delaplane [d], Yongqiang Cheng [c], Roman V. Denys [d], Anibal J. Ramirez-Cuesta [c], Volodymyr A. Yartys [d,∗∗]

[a] *Materials, Chemical, and Computational Science Directorate, National Renewable Energy Laboratory, Golden, CO 80401, USA*
[b] *NIST Center for Neutron Research, National Institute of Standards and Technology, Gaithersburg, MD 20899, USA*
[c] *Oak Ridge National Laboratory, Neutron Spectroscopy Division, Spallation Neutron Source, Oak Ridge TN 37831, USA*
[d] *Institute for Energy Technology, 2027 Kjeller, Norway*
[e] *Department of Materials Science and Engineering, University of Maryland, College Park, MD 20742, USA*
[f] *Department of Chemical Engineering, University of Delaware, Newark, DE 19716, USA*

## ARTICLE INFO

## ABSTRACT

Intermetallic metal hydrides are critical materials for hydrogen storage applications, however, metal hydrides with greater storage capacities are still needed. Within metal hydrides, the volumetric storage capacities are limited by the number of hydrogen-accommodating interstitial sites which can be simultaneously occupied given a minimum hydride nearest-neighbor distance of ≈ 2.1 Å, according to the Switendick-Westlake criterion. To date, violations of this criterion are rare. Perhaps the most well studied compounds violating this criterion are the $R$NiInH$_x$ compounds ($R$ = Ce, La, Nd). Previous neutron diffraction studies on the deuterated species revealed the presence of Ni–D⋯D–Ni–D⋯D–Ni chains with anomalously close D⋯D contacts of ≈ 1.6 Å. Yet there are no neutron vibrational spectroscopic investigations reported for these atypical hydrides. Here we use neutron vibrational spectroscopy (NVS) measurements to probe the hydrogen dynamics in LaNiInH$_x$ ($x$ = 0.67, 1.6) and CeNiInH$_{1.4}$. For $x$ > 0.67, the presence of close H⋯H contacts yields two related features in the vibrational spectrum centered near ≈ 90 meV corresponding to the oscillations of paired H atoms simultaneously occupying neighboring $R_3$Ni tetrahedra. Notably, these features are energetically distinct from comparable vibrational motions for "unpaired" H atoms when $x$ ≤ 0.67. To compare, we also present powder neutron diffraction and NVS measurements for the newly characterized, chemically similar Sn compounds CeNiSnH, CeNiSnH$_2$, and CeNiSnD$_2$. These compounds also contain $R_3$Ni tetrahedra, however, the H-occupied tetrahedra are well separated from each other with the closest H⋯H distances exceeding 2.1 Å, and the Switendick-Westlake criterion is not violated. Consequently, the spectral signature of the close H⋯H contacts is absent in these hydrides.

Published by Elsevier B.V.
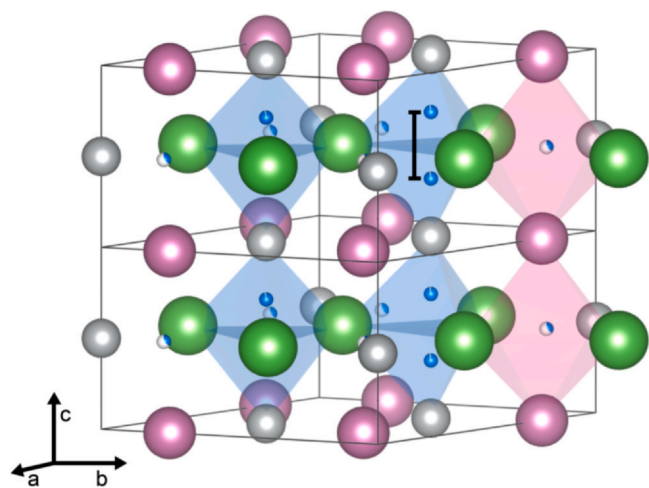CC_BY_4.0

## 1. Introduction

Hydrogen is emerging as a key renewable energy carrier in the push towards a decarbonized energy economy [1]. Yet, the widespread adaptation of hydrogen in energy systems is hindered by a lack of suitable storage materials for both stationary and mobile applications [2,3]. One promising class of materials for hydrogen storage applications are the metal hydrides, which chemisorb molecular hydrogen and store the H atoms in the interstices of the metal lattice [4]. Currently, the best metal hydride materials suffer from low reversible hydrogen storage capacities at operationally relevant conditions [5,6]. Although the volumetric capacity in metal hydrides is high—exceeding that of liquid H$_2$ in many cases [7]—it is

fundamentally limited based on an empirical rule known as the Switendick-Westlake criterion [8,9]. This criterion defines a minimum threshold distance between the hydrogen atoms within structures of metal hydrides of ≈ 2.1 Å. This minimum threshold distance arises from H⋯H coulombic repulsion [10]. The volumetric capacity of H in metal hydrides at operationally relevant conditions can be increased if the Switendick-Westlake criterion could be rationally overcome to increase the volumetric density of H atoms in the metal lattice.

Powder neutron diffraction (PND) studies of intermetallic hydrides have shown that, in practice, the number of available interstices is significantly higher than the number of occupied interstices. As the hydrogen loading increases, the available interstices are either

filled statistically, with occupancies not exceeding ½, or they are filled in an ordered way. For an ordered filling of the sites, the thermodynamically most favorable interstices that first become occupied by H atoms can block nearby sites from filling, via coulombic interactions. Consequently, one important observation is that tetrahedral interstices which share a common face, are never simultaneously filled by H atoms because the distances between their centers are below 2.1 Å, in accordance with the Switendick-Westlake criterion. One typical example is the cubic $AB_2$ Laves-phase family of intermetallic compounds [11,12]. This structure type contains 17 interstitial sites per $AB_2$ unit, including 12 $A_2B_2$ sites, 4 $AB_3$ sites, and 1 $B_4$ site. Yet, the maximum observed stoichiometry of the hydride is 6 absorbed H atoms per $AB_2$ unit, as in $ZrV_2D_6$ (3 $Zr_2V_2$ + 3 $ZrV_3$ sites occupied) [13–15]. At lower hydrogen content, H atoms form ordered superstructures, as in $ZrV_2D_4$ (4 $Zr_2V_2$ sites / $ZrV_2$ unit occupied) [16]. Hydrogen ordering results in H···H contacts exceeding 2 Å.

Very few known compounds to date have displayed unambiguous H···H contacts closer than 2 Å. These include $Th_2AlH_x$ [17–20] and a series of $RNiInH_x$ hydrides ($R$ = La, Ce, Nd, Pr) [21–27]. The $RNiInH_x$ ($0 < x < \sim 1.6$) compounds crystallize in the hexagonal $P\bar{6}2m$ space group (hexagonal ZrNiAl structure type) with hydrogen (deuterium) atoms preferentially filling the $R_3Ni$ tetrahedra (4$h$ crystallographic sites) below $x \approx 1.33$. Prior PND studies of the deuterided $RNiInD_x$ compounds [28] indicated that, as the deuterium loading increases above $x = 0.67$, both $R_3Ni$ interstices of the $NiR_3Ni$ trigonal bipyramids begin to become simultaneously occupied to form close D···D contacts in the metal lattice. Such close pairings are ideally maximized at full $R_3Ni$-site occupation ($x = 1.33$). These D···D contact distances are 1.635(8) Å, 1.606(6) Å, 1.562(9) Å, and 1.570(8) Å for $LaNiInD_{1.22}$, $CeNiInD_{1.24}$, $NdNiInD_{1.19}$, and $NdNiInD_{1.23}$, respectively (values in parentheses here and throughout represent 1σ) [28]. In the La congener, as the loading increases above $x = 1.33$, an additional interstice, the 12$l$ Wyckoff site located within $La_3NiIn_2$ distorted octahedra, becomes populated (although there are indications that these sites can begin to fill before the 4$h$ tetrahedral sites are fully occupied). Fig. 1 shows the structure of $LaNiInD_{1.63}$ and highlights the tetrahedral 4$h$ (blue polyhedra) and octahedral 12$l$ (red polyhedra) sites in the structure. As the deuteride concentration

increases to $x = 1.63$, the D···D contact length increases to 1.715(1) Å [29].

First-principles density functional theory (DFT) investigations of the $RInNiH_x$ compounds revealed a possible mechanism enabling the close H···H pairs. Electron localization function calculations showed that, along the Ni–H chains aligned in the (001) direction, the electron density is localized between the Ni and H atoms to form an H–Ni–H bonded fragment with significant electron density polarization directed towards the In and Ni atoms (i.e. away from the $La_3$ face) [30–32]. It was suggested that the shared $R_3$ faces joining adjacent $R_3Ni$ tetrahedra effectively screen the H···H coulombic repulsion, thus enabling the close hydrogen contacts. Yet, further experimental characterization of these materials is still highly desirable to validate the DFT methodology and develop a more precise understanding of the Ni–H, $R$–H, and possible H–H interactions. A deeper understanding of these interactions may help to further shed light on the mechanism by which these compounds violate the Switendick-Westlake criterion. As such, spectroscopic measurements coupled with DFT phonon calculations are needed to corroborate and enhance our current understanding of the bonding interactions in the $RNiInH_x$ metal hydrides.

Here we present neutron vibrational spectroscopy (NVS) measurements coupled with DFT calculations for the compounds $LaNiInH_x$ ($x = 0.67$, 1.6) and $CeNiInH_{1.4}$. We show that, as the hydrogen loading increases to above $x = 0.67$, large changes occur in the vibrational spectra. Aided by the calculations, we identify the vibrational features associated with the close H···H contacts in these metal hydrides. For comparison, we also report for the first time PND and NVS measurements coupled with DFT calculations for the ternary hydrides CeNiSnH, $CeNiSnH_2$ and $CeNiSnD_2$. These materials share some local structural similarities with the $RNiInH_x$ compounds, however they do not show the crystallographic or spectroscopic signatures of close H···H contacts.

## 2. Experimental section

### 2.1. Synthesis of RNiIn and CeNiSn based hydrides/deuterides

The parent $RNiIn$ intermetallic compounds were prepared by arc melting mixtures of the compact pieces of pure elements (purity > 99.9%) followed by annealing at elevated temperatures in an evacuated quartz ampoule according to previously established procedures [28,29,33]. Typically, the single pieces of the annealed samples were transferred to a Sieverts-type system with an autoclave placed in a furnace, activated at high temperatures (573–623 K), and then exposed for a specific period to gaseous $H_2/D_2$ at an appropriate temperature and pressure. For LaNiIn, approximately 1.4 g was exposed to 0.5 MPa $H_2$ at room temperature to form $LaNiInH_{1.6}$. $LaNiInH_{0.67}$ was formed from $LaNiInH_{1.6}$ by removal of the required amount of $H_2$ outgassed from the sample at 473 K followed by cooling to room temperature.

For CeNiSn (TiNiSi-type orthorhombic structure), hydrogenation at 523 K under 5 MPa of $H_2$ gas has been found by X-ray diffraction (XRD) to yield the dihydride $CeNiSnH_2$ (hexagonal, filled ZrBeSi-type structure) (in house studies and [34]). Hydrogen evacuation of the dihydride at this same temperature leads to decomposition towards the monohydride CeNiSnH (orthorhombic, deformed TiNiSi-type structure). In both hydrides, the metal sublattice has a similar structure to the original intermetallic alloy, however, with different degrees of deformation. Here, $CeNiSnH_2$ was prepared by heating 6 g of CeNiSn at 500 K under 3.5 MPa $H_2$ gas for 20 h. An analogous procedure using $D_2$ yielded $CeNiSnD_2$. Finally, a roughly equimolar mixed-phase monohydride + dihydride $CeNiSnH_{1.43}$ sample (53% orthorhombic CeNiSnH + 47% hexagonal $CeNiSnH_2$ based on PND results) was prepared by heating 6 g of CeNiSn at 650 K under 0.4 MPa $H_2$ gas for 4 h.



**Fig. 1.** Two unit cells of the hexagonal $P\bar{6}2m$ crystal structure for $LaNiInD_{1.63}$ are shown stacked in the (001) direction. Octahedral and tetrahedral coordination environments for the D atoms are highlighted as the red and blue polyhedra, respectively. For clarity, only one column of octahedral polyhedra is shown. The Ni–D···D–Ni–D···D–Ni chains containing the close D···D contacts between neighboring $La_3Ni$ tetrahedral sites run in the (001) direction along the $La_3N_2$ chains. The close D···D contact between adjacent $La_3Ni$ tetrahedra is highlighted by a bold scale bar, indicating a separation of 1.715(1) Å. Gray, green, pink, and blue spheres depict Ni, La, In, and D atoms, respectively, while partial shading denotes occupancy. Figure adapted from reference [29].

## 2.2. Powder neutron diffraction measurements of CeNiSnH$_x$

PND patterns for samples of CeNiSnH$_2$, CeNiSnD$_2$, and CeNiSnH$_{1.43}$ were collected at 295 K using the high-resolution R2D2 instrument ($\lambda$ = 1.551(1) Å, 2$\Theta$ step = 0.05°) at the R2 Reactor at the Studsvik Neutron Research Laboratory, Uppsala University, Sweden (Figs. S6–S8). The instrument calibration parameters and wavelength of the neutron beam were determined by a least-squares fit for diffraction data collected for the standard reference materials; Si, NIST 640c and Al$_2$O$_3$, NIST 676. The samples were loaded in a vanadium sample can (inner diameter = 6 mm). The Pawley [35] and Rietveld [36] refinements of the structure parameters were performed with the GSAS/EXPGUI program package [37].[1]

## 2.3. Neutron vibrational spectroscopic measurements

The neutron vibrational spectra for the LaNiInH$_{0.67}$ and LaNiInH$_{1.6}$ compounds were collected at the National Institute of Standards and Technology Center for Neutron Research (NCNR) using the BT-4 Filter Analyzer Neutron Spectrometer (FANS) [38]. To collect these spectra, horizontal 20′ collimations were used before and after the Cu(220) monochromator to collect higher-resolution data in a neutron energy loss range from 33 meV ($\approx$ 266 cm$^{-1}$) to 160 meV ($\approx$ 1290 cm$^{-1}$). Additional lower-resolution spectra in a neutron energy loss range from 33 meV ($\approx$ 266 cm$^{-1}$) to 256 meV ($\approx$ 2064 cm$^{-1}$) were collected by employing horizontal 60′ and 40′ collimations before and after the monochromator (Figs. S1, S2 in the Supplemental Information document). Because of the large neutron absorption cross section of In ($\approx$ 194 b) [39], the samples were measured as flat plates in a reflectance geometry to enhance scattering signal.

The neutron vibrational spectra for CeNiInH$_{1.4}$ and for the CeNiSnH$_x$ compounds were collected using the high-resolution broadband TOSCA spectrometer at the pulsed neutron source of ISIS at the Rutherford-Appleton Laboratory in Chilton, the United Kingdom (Figs. S3–S5). In an inert atmosphere, the samples were loaded into flat aluminum sample holders and data were collected at 20 K.

## 2.4. Density functional theory calculations

Density Functional Theory (DFT) calculations were performed using the Vienna Ab initio Simulation Package (VASP) [40]. The calculations used the Projector Augmented Wave (PAW) method [41,42] to describe the effects of core electrons, and Perdew-Burke-Ernzerhof (PBE) [43] implementation of the Generalized Gradient Approximation (GGA) for the exchange-correlation functional. The energy cutoff was 600 eV for the plane-wave basis of the valence electrons. The total energy tolerance for the electronic energy minimization was 10$^{-8}$ eV. After structural optimization, a supercell (2 × 2 × 3 of the unit cell except for CeNiSnH, for which it was 3 × 3 × 2) was used for the phonon calculations. The vibrational eigen-frequencies and modes were then calculated by solving the force constants and dynamical matrix using Phonopy [44]. The OCLIMAX software [45] was used to convert the DFT-calculated phonon results to the simulated NV spectra. The DFT calculations for all spectra were conducted using both lattice-dynamics (LD) and molecular-dynamics (MD) approaches. The simulated spectra based on the calculations arise from sampling the entire Brillouin zone. Based on the calculated Γ-point phonons, animations depicting the

atomic motion for each mode were generated and these animations were used to facilitate mode assignments for the measured spectra. These animations—included as .phonon files in the Supplementary Material Data—can be visualized using the Jmol software package [46]. For LaNiInH$_{0.6}$, an ordered singlet model was used for the calculations in which each Ni atom was paired with one H atom such that the Ni–H bonds all pointed uniformly in the positive c-axis crystallographic direction. An additional doublet model which assumed an ordered structure of half-filled 4 h Wyckoff positions, but with only H–Ni–H pair configurations present, was also used for the calculations. Since the simulated spectrum using this model resulted in poor agreement with the measured spectrum and its DFT-predicted potential energy (per H atom) was 0.32 eV higher than that for the singlet structure, it was not considered further. As such, the results discussed below are based on the calculations performed using the ordered singlet model for LaNiInH$_{0.6}$. In all LD simulations, the DFT calculated energy bands are scaled to align with the corresponding peak positions in the measured INS spectra, and the scaling constant ranges from 0.9 to 1.1 (mostly within 1% ± 5%). In addition, MD simulations were performed to better understand anharmonic effects. For example, strong anharmonicity is observed for the three rattling modes of the hydrogen atom at the 12 l octahedral site in LaNiInH$_{1.6}$. The peak positions are nicely reproduced by the MD simulation whereas they are substantially overestimated by the LD simulation. On the other hand, the MD approach tends to produce broader peaks, and the LD simulation reproduces the peak profile (such as the splitting) better, as observed in Fig. 2. As such, we use the animations associated with the calculations for the LaNiInH$_{1.33}$ compound to describe the split modes centered near 92 meV in the measured spectrum for LaNiInH$_{1.6}$. For the octahedral H modes in the measured spectrum for LaNiInH$_{1.6}$, we use the animation for the corresponding feature in the simulated spectrum for LaNiInH$_{1.6}$. Lattice dynamics DFT calculations were sufficient for the CeNiSnH$_x$ compounds.

## 3. Results and discussion

### 3.1. Neutron vibrational signatures of close H⋯H contacts

The neutron-fast-background-corrected vibrational spectra for LaNiInH$_x$ ($x$ = 0.67, 1.6) and for CeNiInH$_{1.4}$ are shown in Fig. 2 along with the simulated spectra for LaNiInH$_x$ ($x$ = 0.67, 1.33, 1.6) and CeNiInH$_{1.6}$. Below we detail the features in each spectrum, and, aided by the DFT calculations, we give assignments for each observed mode. The mode positions and assignments are tabulated in Table 1. Based on the calculated animations, we identify dynamic motions for the H atom at the 4 h Wyckoff sites which are either orthogonal to the basal $R_3$ plane in the $R_3$Ni tetrahedra (Ni–H stretching modes) or parallel to the basal plane (which we term 'bending' and 'rocking' modes). We note that, in true molecular bending and rocking modes, the Ni–H distances would be constant, and the H atoms would move in a sweeping motion. Here, the H atom moves parallel to the $R_3$ face, such that the Ni–H distances vary slightly as the H atoms vibrate. As such, we use the terms 'bending' and 'rocking' in the following discussion as purely descriptive terms to differentiate between the types of motions of the H atoms within a single H–Ni–H bonded fragment, and the quotation marks around the terms will not be used hereafter.

The crystal structure of LaNiInD$_{0.48}$ was shown to contain one occupied hydrogen atom position, the 4 h site, with an occupancy of 0.36 such that there are no close D⋯D contacts in violation of the Switendick-Westlake criterion at this loading concentration [26]. The neutron vibrational spectrum for the analogous LaNiInH$_{0.67}$ contains two narrowly split features at neutron energy loss values of 120.7(5) meV ($\approx$ 974 cm$^{-1}$) and 126.9(5) meV ($\approx$ 1024 cm$^{-1}$) and a broad band extending from $\approx$ 80 to 106 meV ($\approx$ 645 cm$^{-1}$ to
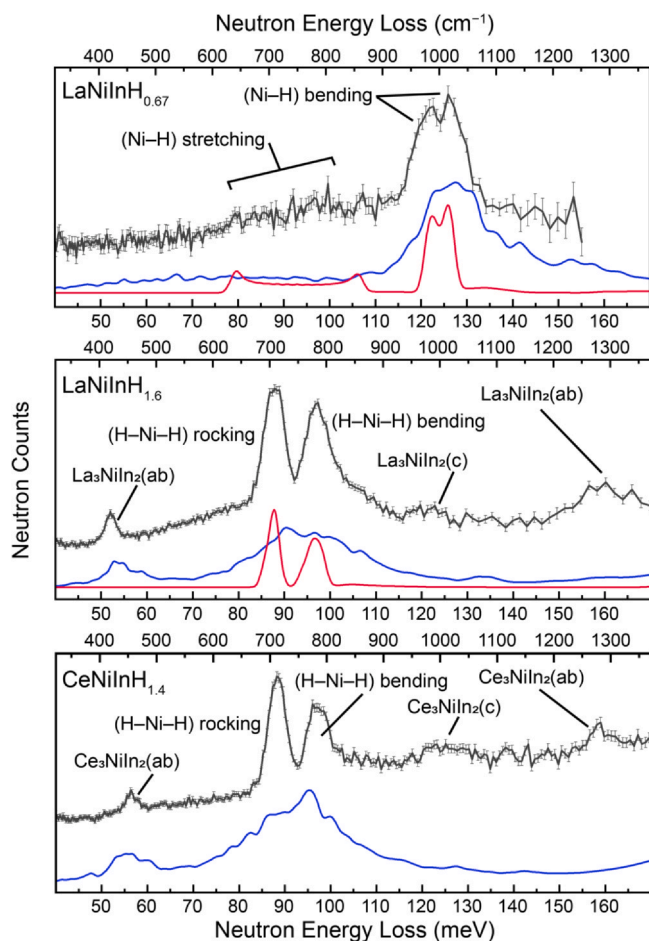
**Fig. 2.** The neutron vibrational spectra for LaNiInH$_{0.67}$ (top), LaNiInH$_{1.6}$ (middle), and CeNiInH$_{1.4}$ (bottom). The measured spectra for LaNiInH$_{0.67}$, LaNiInH$_{1.6}$, and CeNiInH$_{1.4}$ are depicted by the gray curves. LD-based and MD-based simulated spectra (red and blue curves, respectively) for the La congener are plotted with arbitrary offsets below the measured spectra. Note that the LD-based spectrum shown beneath the measured LaNiInH$_{1.6}$ spectrum corresponds to the calculation conducted for LaNiInH$_{1.33}$. The MD-based spectrum for CeNiInH$_{1.6}$ (blue curve) is plotted with an arbitrary offset underneath the measured spectrum for CeNiInH$_{1.4}$. Anharmonic effects arising for the H atoms occupying the octahedral sites smear the otherwise sharp features in the simulated spectra at high hydrogen loadings. Mode assignments are shown next to each feature. Vertical error bars accompanying the measured spectra represent $\pm 1\sigma$.

855 cm$^{-1}$). From the LD DFT calculations using the ordered singlet structural model described above, animations of the modes for the features in the simulated spectra were generated (see the *.phonon* files included with the Supplemental Materials). Based on these animations, the observed spectral features at 120.7(5) meV and 126.9(5) meV reflect two narrowly split Ni–H bending modes corresponding to correlated motions of the hydrogen atoms orthogonal

to the La$_3$ faces. The weaker broad band ranging from $\approx 80$–106 meV reflects $\nu$(Ni–H) stretching motions: an in-phase $\nu$(Ni–H) stretching frequency is calculated to occur at $\approx 106$ meV ($\approx 856$ cm$^{-1}$) and an out-of-phase $\nu$(Ni–H) stretching mode is calculated to occur at $\approx 108$ meV ($\approx 867$ cm$^{-1}$). The unusually broad dispersion of the stretching mode energies in the simulated spectrum shown in Fig. 2 (top) extending down to 80 meV matches well the behavior seen in the experimental spectrum and arises from sampling the entire Brillouin zone. In contrast, the distinct normal-mode energies for the animations are associated with the phonons calculated at the $\Gamma$-point only.

The MD DFT calculations for LaNiInH$_{0.6}$ revealed relatively complex behavior for the H atoms in the $4h$ Wyckoff sites at low temperature. The calculations showed an inherent instability in the singlet structural model resulting in imaginary modes towards the zone boundary in the [0,0,z] direction. This instability is manifested by the H atoms rattling/jumping between adjacent $4h$ sites within the same NiLa$_3$Ni trigonal bipyramidal set of interstices even at very low temperature. This dynamic motion of the H atoms at low temperature reflects significant anharmonicity and low energy barrier between the adjacent $4h$ sites. The complex potential energy profile leads to the significant dispersion observed for the $\nu$(Ni–H) stretching modes. Future quasielastic/inelastic neutron scattering measurements to probe lower-energy excitations may reveal further details.

For LaNiInD$_{1.63}$, the $4h$ tetrahedral site was found to be nearly fully occupied, thus forming close H···H pairs and violating the Switendick-Westlake criterion [29]. At the same time, the octahedral site at the $12l$ Wyckoff position was found to be partially occupied with an occupancy of 0.36. The neutron vibrational spectrum for the analogous LaNiInH$_{1.6}$ compound shows significant differences compared to the spectrum for the $x = 0.67$ compound. The narrowly split $\delta$(H–Ni–H) bending modes at 120.7(5) meV and 126.9(5) meV are absent, and three new features are observed at 52.1(1) meV ($\approx 420$ cm$^{-1}$), 87.68(9) meV ($\approx 707$ cm$^{-1}$), and 97.0(1) meV ($\approx 782$ cm$^{-1}$). These modes correspond to bending, (H–Ni–H) rocking, and $\delta$(H–Ni–H) bending modes, respectively. Note that here we define the mode assignment with respect to the H–Ni–H bonded fragments in the Ni–H···H–Ni–H···H–Ni chains (Table 2).

The two modes centered around $\approx 92$ meV correspond to the dynamic motions of H atoms in the close H···H pairs and represent the key vibrational spectral signature for close H···H contacts in this $R_3$Ni environment below 200 meV. The hydrogen atom motions associated with these (H–Ni–H) rocking and $\delta$(H–Ni–H) bending modes are parallel to the La$_3$ basal plane in the La$_3$Ni tetrahedra. The animations generated from the calculations indicate that the rocking mode at 87.68(9) meV corresponds to degenerate rocking motions of the H–Ni–H bonded fragments which are all rocking in-phase within the individual H–Ni–H···H–Ni–H columns in the (001) crystallographic direction, but out-of-phase with respect to the H–Ni–H motions in the neighboring columns. Here, the close H···H atoms in adjacent La$_3$Ni tetrahedra, within the same NiLa$_3$Ni trigonal

**Table 1**
$d$(Ni–H) and $d$(H···H) distances are tabulated along with the measured neutron energy loss values in meV for the assigned modes associated with the tetrahedrally coordinated H atoms.

| Hydride | $d$(Ni–H) (Å) | $d$(H···H) (Å) | (Ni–H) 'bending' (meV) | | $\nu$(Ni–H) stretching (meV) |
|---|---|---|---|---|---|
| LaNiInH$_{0.67}$ | 1.68(1)[a] | – | 120.7(5), 126.9(5) | | $\approx 80$–106 (band) |
| CeNiSnH | 1.626(6) | 2.66(1) | 102.01(3), 118.91(2) | | 156.21(5) |
| | | | (H–Ni–H) 'rocking' (meV) | $\delta$(H–Ni–H) 'bending' (meV) | $\nu$(H–Ni–H) stretching (meV) |
| LaNiInH$_{1.6}$ | 1.494(6)[b] | 1.715(1)[b] | 87.68(9) | 97.0(1) | 209, 230 (calc.) |
| CeNiInH$_{1.4}$ | 1.509(3)[a] | 1.606(6)[a] | 88.29(4) | 97.00(7) | – |
| CeNiSnH$_2$ | 1.633(3) | 2.76(1) | – | 85.93(4) | 140.63(4) |

'Bending' and 'rocking' refer to H || R3 motion in the R3Ni tetrahedra as described in the text. Values in parentheses indicate $\pm 1\sigma$
[a] Contact distances for LaNiInH$_{0.67}$ and CeNiInH$_{1.4}$ based on crystal structures for LaNiInD$_{0.48}$ and CeNiInD$_{1.24}$, respectively [28].
[b] Contact distances for LaNiInH$_{1.6}$ based on the crystal structure for LaNiInD$_{1.63}$ [29].

**Table 2**

Crystallographic parameters for CeNiSnH ($Pna2_1$, $a = 7.2804(5)$, $b = 8.4883(5)$, $c = 4.4064(3)$ Å; $V = 272.31(2)$ Å$^3$), CeNiSnH$_2$ ($P6_3/mmc$, $a = 4.3956(1)$, $c = 8.5475(3)$ Å; $V = 143.020(5)$ Å$^3$), and CeNiSnD$_2$ ($P6_3/mmc$, $a = 4.3947(2)$, $c = 8.5329(4)$Å; $V = 142.72(1)$ Å$^3$).

| CeNiSnH$_{0.97(1)}$ | W. | $x$ | $y$ | $z$ | $U_{iso}$ (Å$^2$) |
|---|---|---|---|---|---|
| Ce | $4a$ | 0.0104(6) | 0.3088(4) | 0.237(6) | 1 |
| Ni | $4a$ | 0.7821(3) | 0.8995(2) | 0.230(3) | 1 |
| Sn | $4a$ | 0.6607(4) | 0.5674(5) | 0.232(4) | 1 |
| H | $4a$ | 0.4404(8) | 0.089(1) | 0.709(4) | 2 |
| CeNiSnH$_{1.74(4)}$ | W. | $x$ | $y$ | $z$ | $U_{iso}$ (Å$^2$) |
| Ce | $2a$ | 0 | 0 | 0 | 0.81(5) |
| Ni | $2c$ | $^1/_3$ | $^2/_3$ | $^1/_4$ | 0.74(4) |
| Sn | $2d$ | $^2/_3$ | $^1/_3$ | $^1/_4$ | 0.70(6) |
| H | $4f$ | $^1/_3$ | $^2/_3$ | 0.0589(3) | 2.7(1) |
| CeNiSnD$_2$ | W. | $x$ | $y$ | $z$ | $U_{iso}$ (Å$^2$) |
| Ce | $2a$ | 0 | 0 | 0 | 1.04(8) |
| Ni | $2c$ | $^1/_3$ | $^2/_3$ | $^1/_4$ | 1.15(5) |
| Sn | $2d$ | $^2/_3$ | $^1/_3$ | $^1/_4$ | 0.81(8) |
| D | $4f$ | $^1/_3$ | $^2/_3$ | 0.0607(2) | 2.34(6) |

Values in parentheses indicate ± 1σ. 'W.' in the second column denotes Wyckoff position. Note a small isotopic effect on a replacement of H by D in CeNiSnH(D)$_2$ with a small contraction of the lattice for the dideuteride as compared to the dihydride.

bipyramid, move out-of-phase with each other. In contrast, the bending mode at 97.0(3) meV corresponds to degenerate correlated bending motions of the (H–Ni–H) moieties which are in-phase both within and between the NiLa$_3$Ni columns in the (001) crystallographic direction. The close H···H atoms in adjacent La$_3$Ni tetrahedra move in-phase with each other (see *.phonon* files included with the Supplemental Materials). Hence it is clear that the narrowly split bending modes at 120.7(5) meV and 126.9(5) meV in LaNiInH$_{0.67}$ significantly red-shift and further split in LaNiInH$_{1.6}$ as the close H···H contacts form.

The simulated spectrum for LaNiInH$_{1.6}$ also contains the in-phase and out-of-phase $\nu_{sym}$(Ni–H) symmetric stretching modes at significantly higher neutron energy loss values of $\approx 209$ meV ($\approx 1690$ cm$^{-1}$) and $\approx 231$ meV ($\approx 1830$ cm$^{-1}$), respectively. For the in-phase modes, the close H···H atoms vibrate with each other whereas for the higher-energy mode, these atoms vibrate against each other. These values are out of the measured spectral window for the high-resolution measurement shown in Fig. 2 and are unfortunately not well resolved by the higher-energy, low-resolution measurement shown in Fig. S2.

Weaker modes at 52.1(1) meV, 122.0(5) meV, and 158.6(5) meV correspond to the three normal-mode vibrations of the hydrogen atoms filling the La$_3$NiIn$_2$ distorted octahedra. The modes at 52.1(1) meV and 158.6(5) meV represent orthogonal vibrations of the H atom within the equatorial La$_3$Ni plane, whereas the mode at 122.0(5) meV corresponds to motions of this atom in the *c*-axis direction along the In–H–In axis. These motions are associated with minimal accompanying motion from the hydrogen atoms at the $4h$ site (see *.phonon* files included as Supplemental Materials).

The measured spectrum for CeNiInH$_{1.4}$ is also shown in Fig. 2. The two features indicative of close H···H contacts are also prominent in this spectrum. The features for the (H–Ni–H) rocking and δ(H–Ni–H) bending modes appear at neutron energy loss values of 88.29(4) meV ($\approx 712$ cm$^{-1}$), and 97.00(7) meV ($\approx 782$ cm$^{-1}$), respectively. Given the structural similarity in the $R_3$Ni ($R$ = La, Ce) tetrahedra between LaNiInH$_{1.6}$ and CeNiInH$_{1.4}$, these modes remain at nearly the same energy loss values between the two compounds. The slight differences in energy for the modes may arise from the slightly longer La–Ni bonds in LaNiInH$_{1.225}$ (3.2445(8) Å) compared to CeNiInH$_{1.236}$ (3.2128(11) Å), [28] leading to slightly less confined H atoms and therefore slightly lower energy modes in the La congener. Unfortunately, similar to the LaNiInH$_{1.6}$ case, the $\nu$(Ni–H) stretching frequencies for CeNiInH$_{1.4}$ above 200 meV are also not well resolved in the higher-energy, high-resolution measurement shown in Fig. S3,

likely due to factors including overlapping combination bands in this energy range, inadequate statistics, and mode dispersion.

A slight increase is apparent in the neutron energy loss values for the H rattling modes in the Ce$_3$NiIn$_2$ octahedra compared to the La$_3$NiIn$_2$ octahedra. The modes blue-shift slightly from 52.1(1) meV, 122.0(5) meV, and 158.6(5) meV in the La congener to 56.4(2) meV, 123.9(8) meV, and 158.7(3) meV in the Ce compound, respectively. These shifts may arise from a slightly stronger $R$–H interaction in the Ce compound at the $12l$ octahedral site stemming from a slightly larger Pauling electronegativity value for Ce (1.12) than for La (1.1) (H Pauling electronegativity = 2.2) [47].

### 3.2. Comparison to structurally and chemically similar CeNiSnH$_x$ hydrides

As a comparison to the $R$NiInH$_x$ compounds, we synthesized and studied the CeNiSnH$_x$ ($x$ = 1; 2) hydrides. Earlier, the Ce$_3$Ni tetrahedra in CeNiSnH$_2$ were hypothesized as the most likely hydrogen sites based on XRD measurements [48]. However, these sites in CeNiSnH$_2$ have never been crystallographically identified by neutron diffraction measurements. Here, we present PND measurements of CeNiSnD$_2$, CeNiSnH$_2$, and CeNiSnH$_{1.43}$ (mixed sample of the $x$ = 1 and $x$ = 2 compounds). The PND measurements of the CeNiSnH$_{1.43}$ sample indicate a mixture of CeNiSnH$_x$ with 53% of the monohydride, $x$ = 0.97(1) and 47% of the dihydride, $x$ = 1.94(2) (yielding an overall $x$ = 1.43). We find that these compounds crystallize in the $Pna2_1$ ($x$ = 1) and the $P6_3mmc$ ($x$ = 2.0) space groups, in agreement with the earlier diffraction measurements (Figs. S6–S8) [34,49]. In the $x$ = 2 compound, the D atoms indeed occupy the Ce$_3$Ni interstitial sites, as suggested earlier based on the structure of the analogous LaNiSnD$_2$ compound [48]. A significant difference in CeNiSnD$_2$ (Fig. 3b) compared to CeNiInD$_{1.236}$ (Fig. 3c) is that every other Ni atom in the Ni–H···H–Ni–H···H–Ni chain is substituted with a Sn atom. The $R_3$-face-sharing of adjacent $R_3$Ni tetrahedra is replaced by $R_3$-face-sharing between adjacent Ce$_3$Ni and Ce$_3$Sn tetrahedra, forming NiCe$_3$Sn trigonal bipyramids. Deuterium (hydrogen) occupation of the Ce$_3$Sn tetrahedra is not observed in the structure, and chains of Ni–H⟦⟧·Sn⟦⟧·H–Ni run in the (001) crystallographic direction (where ⟦⟧ denotes the lack of an H atom, because the Sn atoms do not form chemical bonds in the (001) direction; Fig. 3b). Because the Ce$_3$Sn tetrahedra are not occupied by D atoms, the Switendick-Westlake criterion is not violated in the CeNiSnH$_x$ compounds.

The neutron vibrational spectra measured for CeNiSnH$_{1.43}$ and CeNiSnH$_2$ are shown in Fig. 4 together with the corresponding simulated phonon spectrum based on the DFT calculations. The neutron vibrational spectrum measured for CeNiSnH$_{1.43}$ is shown in Fig. 4 (top). The modes for CeNiSnH occur at neutron energy loss values of 102.01(3) meV ($\approx 839$ cm$^{-1}$), $\approx 118.91(2)$ meV ($\approx 951$ cm$^{-1}$), and 156.21(5) meV ($\approx 1255$ cm$^{-1}$). Aided by animations of these modes generated from the DFT calculations, we assign these as bending, bending, and $\nu$(Ni–H) stretching modes, respectively. Similarly, for CeNiSnH$_2$, we identify modes at 85.93(4) meV ($\approx 693$ cm$^{-1}$) and 140.63(4) meV ($\approx 1134$ cm$^{-1}$), which we assign as δ(H–Ni–H) bending and $\nu$(Ni–H) stretching modes, respectively. Four nearly degenerate stretching modes are calculated at $\approx 140$ meV: two asymmetric stretching modes and two symmetric stretching modes differentiated by the in-phase or out-of-phase nature of the vibrations of the adjacent H–Ni–H moieties. These modes are calculated to occur at 130.1 meV (asymmetric, in-phase), 140.1 meV (symmetric, out-of-phase), 140.5 (asymmetric, out-of-phase), and 146.1 meV (symmetric, in-phase). Unlike the extensive energy dispersion across the Brillouin zone associated with the Ni–H stretching modes of the $R$NiInH$_x$ compounds, those for the CeNiSnH$_x$ compounds are rather sharp. This may be due to the H-metal alternating arrangement in CeNiSnH$_x$ resulting in a more harmonic and isolated local
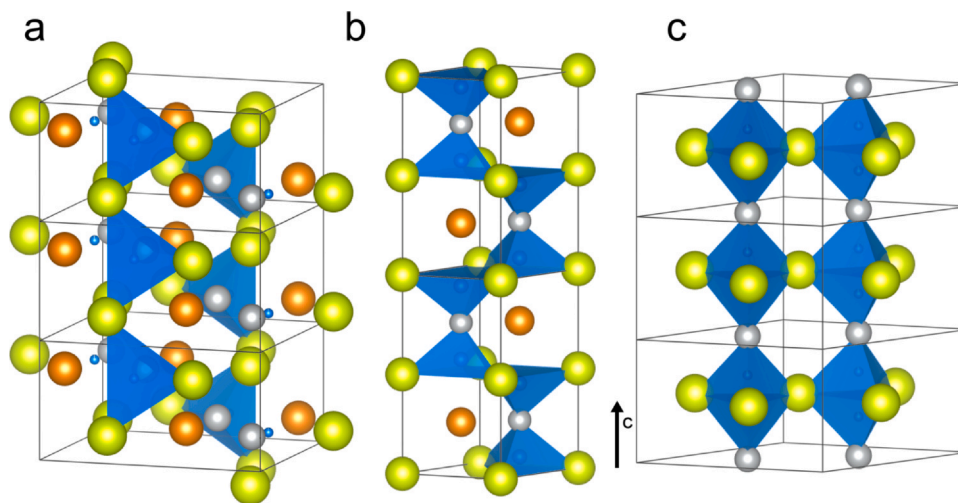
**Fig. 3.** The H(D)-occupied $Ce_3Ni$ tetrahedra are shown for CeNiSnH (a), $CeNiSnD_2$ (b), and $CeNiInD_{1.236}$ (c) [28]. For clarity, only selected chains of $Ce_3Ni$ tetrahedra are shown as polyhedra for CeNiSnH (a), and only a fragment of the $CeNiInD_{1.236}$ compound is shown in (c). Broken and continuous chains of occupied teterahedra run in the (001) crystallographic direction for $CeNiSnD_2$ and for $CeNiInD_{1.236}$, respectively. Yellow, orange, gray, and blue spheres depict Ce, Sn, Ni, and D atoms, respectively.
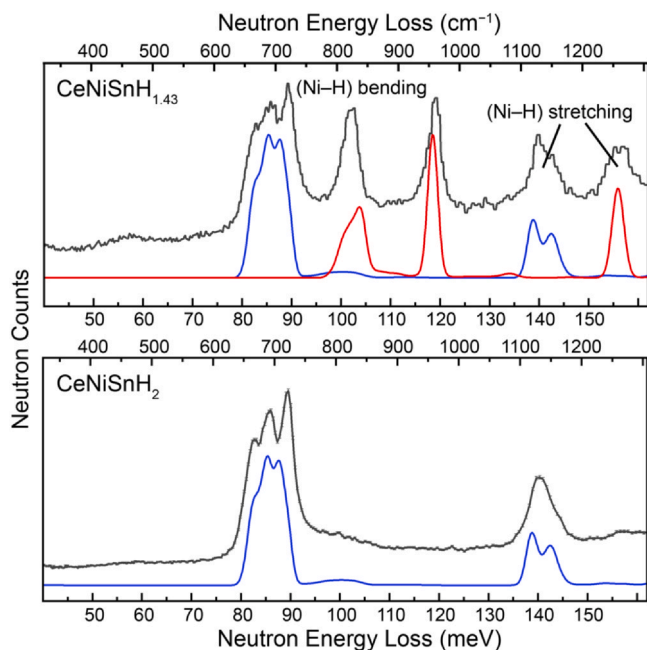


**Fig. 4.** Depicted here are the neutron vibrational spectra (gray curves) for $CeNiSnH_{1.43}$ (above) and $CeNiSnH_2$ (below). The LD-based simulated spectra for CeNiSnH (red curve) and $CeNiSnH_2$ (blue curves) are offset arbitrarily below the measured spectra. Above, the combination of the simulated spectra give successful qualitative agreements with the measured spectrum. Full measured spectral windows are shown in Figs. S4 and S5. Mode assignments are given next to each feature (above).

environment around H, such that their vibrational behavior is better defined and more independent. In contrast, the two adjacent filled $4h$ sites in $LaNiInH_x$ lead to complex H interactions with itself and its neighbors, thus the vibrational frequencies are more sensitive to the surrounding atoms, generating more dispersion. The spectral signatures for the close H⋯H contacts are absent in the $CeNiSnH_x$ compounds, as expected based on the neutron diffraction-derived structures presented herein.

The modes corresponding to the dynamic motions of the hydrogen atoms in the $Ce_3Ni$ tetrahedra in $CeNiSnH_2$ can be compared to the modes for the H atoms in the $La_3Ni$ tetrahedra in $LaNiInH_{0.67}$. The three modes in the measured spectral window for $LaNiInH_{0.67}$

are the $\nu$(Ni–H) stretching mode corresponding to the broad band from ≈ 80–106 meV and the two δ(H–Ni–H) narrowly split bending modes at 120.7(5) meV and 126.9(5) meV. In $CeNiSnH_2$, the bending and stretching modes occur at 85.93(4) meV and 140.63(4) meV, respectively. The bending mode is red-shifted by ≈ 40 meV while the stretching frequency is blue-shifted by ≈ 50 meV in the Ce compound compared to the La compound. These changes in energy may arise due to tighter confinement of the H atoms due to a smaller $La_3$ face in the $R_3Ni$ tetrahedra. The La–La distance is ≈ 4.05 Å compared to a Ce–Ce distance ≈ 4.40 Å, leading to the polyhedral volumes of ≈ 4.81 Å$^3$ and ≈ 5.95 Å$^3$, respectively).

## 4. Conclusions

In conclusion, we report here for the first time the vibrational spectroscopic signature associated with H atoms with close H⋯H contacts in violation of the Switendick-Westlake criterion in a metal hydride. We investigated the compounds $RNiInH_x$ ($R$ = La, $x$ = 0.67, 1.6; $R$ = Ce, $x$ = 1.4), which contain close H⋯H contacts in face-sharing $R_3Ni$ tetrahedra above $x$ = ⅔. We studied these compounds using NVS measurements coupled with DFT calculations. Assisted by the simulated spectra based on these calculations, we assign the observed spectral modes for these compounds. The two $RNiInH_x$ metal hydrides studied here for $R$=La display two modes in the neutron vibrational spectra which arise from the basal plane H atom vibrations in the $R_3Ni$ tetrahedra. As the loading increases above $x$ = ⅔, the Switendick-Westlake criterion is violated, and these modes undergo significant softening and increased splitting because of the interaction of the close H atoms in neighboring $R_3Ni$ tetrahedra (d (H⋯H) ≈ 1.6 Å). As a comparison, we also synthesized and studied the structurally similar $CeNiSnH_x$ ($x$ = 1.0, 2.0) compounds using PND and NVS measurements combined with DFT calculations. During the hydrogenation of the CeNiSn intermetallic alloy with a TiNiSi-type orthorhombic structure, two hydrides are formed, a monohydride CeNiSnH (orthorhombic, deformed TiNiSi type structure) and a dihydride $CeNiSnH_2$ (hexagonal, filled ZrBeSi type). These compounds do not display the structural or spectroscopic signatures of close H⋯H contacts. We envision that the results presented herein will aid future characterization of metal hydrides using NVS measurements and may help guide the effort towards developing new metal hydride species with enhanced hydrogen storage capacities at operationally relevant temperatures.

## Declaration of Competing Interest

The authors declare that they have no known competing financial interests or personal relationships that could have appeared to influence the work reported in this paper.

## Acknowledgements

## Appendix A. Supporting information

Supplementary data associated with this article can be found in the online version at doi:10.1016/j.jallcom.2021.162381.

## References

[1] I. Staffell, D. Scamman, A.V. Abad, P. Balcombe, P.E. Dodds, P. Ekins, N. Shah, K.R. Ward, The role of hydrogen and fuel cells in the global energy system, Energy Environ. Sci. 12 (2019) 463–491.

[2] M. Hirscher, V.A. Yartys, M. Baricco, J. Bellosta von Colbe, D. Blanchard, R.C. Bowman Jr., D.P. Broom, C.E. Buckley, F. Chang, P. Chen, Y.W. Cho, J.C. Crivello, F. Cuevas, W. David, P.E. de Jongh, R.V. Denys, M. Dornheim, M. Felderhoff, Y. Filinchuk, G.E. Froudakis, D.M. Grant, E.M. Gray, B.C. Hauback, T. He, T.D. Humphries, T.R. Jensen, S. Kim, Y. Kojima, M. Latroche, H.W. Li, M.V. Lototskyy, J.W. Makepeace, K.T. Møller, L. Naheed, P. Ngene, D. Noréus, M.M. Nygård, Si Orimo, M. Paskevicius, L. Pasquini, D.B. Ravnsbæk, M. Veronica Sofianos, T.J. Udovic, T. Vegge, G.S. Walker, C.J. Webb, C. Weidenthaler, C. Zlotea, Materials for hydrogen-based energy storage–past, recent progress and future outlook, J. Alloy. Compd. 827 (2020) 153548.

[3] J. Ren, N.M. Musyoka, H.W. Langmi, M. Mathe, S. Liao, Current research trends and perspectives on materials-based hydrogen storage solutions: a critical review, Int. J. Hydrog. Energy 42 (2017) 289–311.

[4] R. Mohtadi, Si Orimo, The renaissance of hydrides as energy materials, Nat. Rev. Mater. 2 (2016) 1–15.

[5] N. Rusman, M.A. Dahari, Review on the current progress of metal hydrides material for solid-state hydrogen storage applications, Int. J. Hydrog. Energy 41 (2016) 12108–12126.

[6] R.A. Klein, H.A. Evans, B.A. Trump, T.J. Udovic, C.M. Brown, Neutron scattering studies of materials for hydrogen storage, Reference Module in Chemistry, Molecular Sciences and Chemical Engineering, Elsevier, 2021, , https://doi.org/10.1016/B978-0-12-823144-9.00028-5

[7] B. Sakintuna, F. Lamari-Darkrim, M. Hirscher, Metal hydride materials for solid hydrogen storage: a review, Int. J. Hydrog. Energy 32 (2007) 1121–1140.

[8] A. Switendick, Band structure calculations for metal hydrogen systems; Sandia Labs., Albuquerque, NM (USA), (1979).

[9] B. Rao, P. Jena, Switendick criterion for stable hydrides, Phys. Rev. B 31 (1985) 6726–6730.

[10] J.F. Halet, J.Y. Saillard, C. Koudou, C. Minot, Z. Nomikou, R. Hoffmann, C. Demangeat, An orbital analysis of hydrogen pairing in nonstoichiometric transition-metal hydrides, Chem. Mater. 4 (1992) 153–161.

[11] D. Shaltiel, I. Jacob, D. Davidov, Hydrogen absorption and desorption properties of AB₂ Laves-phase pseudobinary compounds, J. Less Common Met. 53 (1977) 117–131.

[12] F. Laves, H. Witte, Die Kristallstruktur des MgNi₂ und seine Beziehungen zu den Typen MgCu₂ und MgZn₂, Metallwirtsch 14 (1935) 645–649.

[13] J.-J. Didisheim, K. Yvon, P. Fischer, D. Shaltiel, The deuterium site occupation in ZrV₂Dₓ as a function of the deuterium concentration, J. Less Common Met 73 (1980) 355–362.

[14] J.-J. Didisheim, K. Yvon, D. Shaltiel, P. Fischer, P. Bujard, E. Walker, The distribution of the deuterium atoms in the deuterated cubic laves-phase ZrV₂D₄.₅, Solid State Commun. 32 (1979) 1087–1090.

[15] A. Borgschulte, J. Terreni, E. Billeter, L. Daemen, Y. Cheng, A. Pandey, Z. Łodziana, R.J. Hemley, A.J. Ramirez-Cuesta, Inelastic neutron scattering evidence for anomalous H–H distances in metal hydrides, Proc. Natl. Acad. Sci. U. S. A 117 (2020) 4021–4026.

[16] J.-J. Didisheim, K. Yvon, P. Fischer, P. Tissot, Order-disorder phase transition in ZrV₂D₃.₆, Solid State Commun. 38 (1981) 637–641.

[17] J. Bergsma, J.A. Goedkoop, J. Van, Vucht, Neutron diffraction investigation of solid solutions AlTh₂Dₕ, Acta Crystallogr. 14 (1961) 223–228.

[18] K. Yvon, P. Fischer, Crystal and magnetic structures of ternary metal hydrides: a comprehensive review, Hydrog. Intermet. Compd. I (1988) 87–138.

[19] M. Sørby, H. Fjellvåg, B. Hauback, A. Maeland, V.A. Yartys, Crystal structure of Th₂Al deuterides, J. Alloy. Compd. 309 (2000) 154–164.

[20] P. Vajeeston, R. Vidya, P. Ravindran, H. Fjellvåg, A. Kjekshus, A. Skjeltorp, Electronic structure, phase stability, and chemical bonding in Th₂Al and Th₂AlH₄, Phys. Rev. B 65 (2002) 75101.

[21] M. Sen, A. Ghoshray, K. Ghoshray, S. Sil, N. Chatterjee, Ordered arrangement of proton pairs in the PrNiInH₁.₂₉ system, Phys. Rev. B 53 (1996) 14345–14348.

[22] M. Sen, S. Giri, K. Ghoshray, B. Bandyopadhyay, A. Ghoshray, N. Chatterjee, Study of magnetic susceptibility & lattice parameters of CeNiInHₓ systems, Solid State Commun. 89 (1994) 327–330.

[23] K. Ghoshray, B. Bandyopadhyay, M. Sen, A. Ghoshray, N. Chatterjee, Observation of a Pake doublet in the ¹H nuclear-magnetic-resonance spectrum of CeNiInHₓ, Phys. Rev. B 47 (1993) 8277–8280.

[24] M. Sato, R. Denys, A. Riabov, V.A. Yartys, Thermodynamic properties of the RENiIn hydrides with RE= La, Ce, Pr and Nd, J. Alloy. Compd. 397 (2005) 99–103.

[25] M. Sato, R. Denys, A. Riabov, V.A. Yartys, Influence of Al-and Cu-doping on the thermodynamic properties of the LaNiIn–H system, J. Alloy. Compd. 400 (2005) 184–187.

[26] M. Sato, R. Denys, A. Riabov, V.A. Yartys, Thermodynamic characteristics of the Al-and Cu-doped NdNiIn hydrides, J. Alloy. Compd. 404 (2005) 43–46.

[27] Ł. Gondek, K. Koźlak, J. Czub, D. Rusinek, A. Szytuła, A. Hoser, On the verge of short D–D distances in RNiIn deuterides, Intermetallics 34 (2013) 23–28.

[28] V.A. Yartys, R. Denys, B. Hauback, H. Fjellvåg, I. Bulyk, A. Riabov, Y.M. Kalychak, Short hydrogen–hydrogen separations in novel intermetallic hydrides, RE₃Ni₃In₃D₄ (RE= La, Ce and Nd), J. Alloy. Compd. 330 (2002) 132–140.

[29] R. Denys, A. Riabov, V.A. Yartys, B. Hauback, H. Brinks, In situ powder neutron diffraction study of LaNiInD₁.₆₃ with short D···D distances, J. Alloy. Compd. 356 (2003) 65–68.

[30] P. Ravindran, P. Vajeeston, R. Vidya, A. Kjekshus, H. Fjellvåg, Violation of the minimum HH separation "rule" for metal hydrides, Phys. Rev. Lett. 89 (2002) 106403.

[31] A. Jezierski, B. Penc, A. Szytuła, Electronic structures of LaNiIn and LaNiInHₓ (x = ⅓, ⅔, 1 and ⁴/₃), J. Alloy. Compd. 404 (2005) 204–207.

[32] P. Vajeeston, P. Ravindran, R. Vidya, A. Kjekshus, H. Fjellvåg, V.A. Yartys, Short hydrogen-hydrogen separation in RNiInH1.333 (R = La, Ce, Nd), Phys. Rev. B 67 (2003) 14101.

[33] A. Iandelli, A. Palenzona, Crystal chemistry of intermetallic compounds, Handbook on the Physics and Chemistry of Rare Earths, 2, (1979) 1–54.

[34] F. Weill, M. Pasturel, J.-L. Bobet, B. Chevalier, Ordering phenomena in intermetallic CeMX (M= Ni, Cu and X= Si, Ge, Sn) upon hydrogenation, J. Phys. Chem. Solids 67 (2006) 1111–1114.

[35] G.S. Pawley, Unit-cell refinement from powder diffraction scans, J. Appl. Crystallogr. 14 (1981) 357–361.

[36] H.M. Rietveld, A profile refinement method for nuclear and magnetic structures, J. Appl. Crystallogr. 2 (1969) 65–71.

[37] A. C. Larson, R. B. Von Dreele, General Structure Analysis System (GSAS), Los Alamos National Laboratory Report LAUR, (2000), 86–748.

[38] T.J. Udovic, C.M. Brown, J.B. Leão, P.C. Brand, R.D. Jiggetts, R. Zeitoun, T.A. Pierce, I. Peral, J.R.D. Copley, Q. Huang, D.A. Neumann, R.J. Fields, The design of a bismuth-based auxiliary filter for the removal of spurious background scattering associated with filter-analyzer neutron spectrometers, Nucl. Instrum. Methods A 588 (2008) 406–413.

[39] V.F. Sears, Neutron scattering lengths and cross sections, Neutron News 3 (1992) 29–37.

[40] G. Kresse, J. Furthmüller, Efficient iterative schemes for ab initio total-energy calculations using a plane-wave basis set, Phys. Rev. B 54 (1996) 11169–11186.

[41] P.E. Blochl, Projector augmented-wave method, Phys. Rev. B 50 (1994) 17953–17979.

[42] G. Kresse, D. Joubert, From ultrasoft pseudopotentials to the projector augmented-wave method, Phys. Rev. B 59 (1999) 1758–1775.

[43] J.P. Perdew, K. Burke, M. Ernzerhof, Generalized gradient approximation made simple, Phys. Rev. Lett. 77 (1996) 3865–3868.

[44] A. Togo, I. Tanaka, First principles phonon calculations in materials science, Scr. Mater. 108 (2015) 1–5.

[45] Y.Q. Cheng, L.L. Daemen, A.I. Kolesnikov, A.J. Ramirez-Cuesta, Simulation of inelastic neutron scattering spectra using OCLIMAX, J. Chem. Theory Comput. 15 (2019) 1974–1982.

[46] Jmol: an open-source Java viewer for chemical structures in 3D. ⟨http://www.jmol.org/⟩.

[47] L. Pauling, The Nature of the Chemical Bond, Cornell University Press, Ithaca, NY, 1960.

[48] V.A. Yartys, T. Olavesen, B. Hauback, H. Fjellvåg, H. Brinks, Hexagonal LaNiSnD$_2$ with a filled ZrBeSi-type structure, J. Alloy. Compd. 330 (2002) 141–145.

[49] V.A. Yartys, B. Ouladdiaf, O. Isnard, O. Yu Khyzhun, K.H.J. Buschow, Hydrogen induced antiferromagnetism in the Kondo semimetal CeNiSn, J. Alloy. Compd. 359 (2003) 62–65.